Vibronic coherences in light harvesting nanotubes: unravelling the role of dark states

Journal Name

ARTICLE TYPE

Cite this: DOI: 00.0000/xxxxxxxxxx

Vibronic coherences in light harvesting nanotubes: unravelling the role of dark states†

Sandra Doria,[a,b] Mariangela Di Donato,[a,b] Raffaele Borrelli,*[c] Maxim F. Gelin,[d] Justin Caram,[e] Marco Pagliai,[f] Paolo Foggi,[g,b,h] and Andrea Lapini,*[i,b]

Received Date
Accepted Date

DOI: 00.0000/xxxxxxxxxx

Self assembled ordered structures, such as H- or J- type molecular aggregates of organic chromophores, are extremely interesting materials for different optoelectronic applications.In this work we present a novel characterization of light harvesting nanotubes formed by self-assembling of amphiphilic cyanine dyes in water, through a combined ultrafast spectroscopic and theoretical approach. In the condition of low inhomogeneous disorder at low temperature, broadband transient absorption spectroscopy revealed the presence of an unusual ultrafast behavior of the aggregate, manifested through intense and peculiar oscillations of the kinetic traces, lasting tens of picoseconds. Theoretical simulations were performed by adapting a model which grasps vibronically coherent effects in the double wall nanotube system experiencing inter-wall energy transfer. Good agreement between model predictions and experimental observations were obtained under the assumption of coupling between bright and dark electronic states. The model clarified the vibronic origin of the observed oscillations, evidencing new important pieces of information about transport mechanisms and excitonic interactions in these complex molecular systems.

1 Introduction

Molecular materials with large exciton diffusion lengths, such as self-assembled J-aggregates, can represent an alternative to conventional silicon-based semiconductors for the development of organic thin film transistors or organic photovoltaic solar cells.[1–4] Emissive ordered aggregates of small organic molecules can be furthermore exploited for the development of organic light emitting diods (OLED); the cooperative emissive properties observed for J-aggregates at low temperature (superradiance) have been extensively exploited in several photonic applications.[5,6] Although notable progress has been made in the last ten years in understanding the photophysics of such molecular aggregates,[7,8]succeeding in specifically designing systems with an optimized exciton behavior still requires further experimental and theoretical investigations. Being able to correlate the excitonic properties of aggregate materials with parameters related to the molecular and electronic structure of the monomeric units and their packing, and understand how these properties are sensitive to external perturbations such as disorder and temperature, is extremely important in order to develop improved optical materials. Another crucial question is to uncover microscopic mechanisms and pathways of the energy transfer, with the ultimate goal to harness these mechanisms for the optimization of artificial systems for energy applications. These are the main issues targeted by the present work. Light Harvesting Nanotubes (LHNs) made of strongly packed cyanine dyes, characterized by a high degree of order and exciton diffusion over long distances, are ideal model systems for designing artificial bio-inspired materials for energetic applications and for disentangling the complex exciton dynamics which are typical of photosynthetic systems.[9–12].

Typical features of these materials are narrow spectral lineshapes, high emission quantum yield and large absorption cross-section in the visible and near infrared region, desirable prop-

[a]ICCOM-CNR, via Madonna del Piano 10, I-50019 Sesto Fiorentino (FI), Italy.
[b]LENS (European Laboratory for Non-Linear Spectroscopy), Via N. Carrara 1, 50019 Sesto Fiorentino, FI, Italy.
[c]DISAFA, University of Torino, Largo Paolo Braccini 2, I-10095 Grugliasco (TO), Italy. Email: raffaele.borrelli@unito.it
[d]School of Sciences, Hangzhou Dianzi University, Hangzhou 310018, China.
[e]Department of Chemistry and Biochemistry, University of California, Los Angeles, CA 90095, USA.
[f]Dipartimento di Chimica "Ugo Schiff", Università degli Studi di Firenze, via della Lastruccia 3, I-50019, Sesto Fiorentino, Italy.
[g]Department of Chemistry, Biology and Biotechnology, Centro di Eccellenza sui Materiali Innovativi Nanostrutturati (CEMIN), University of Perugia, via Elce di Sotto 8, Perugia, 06123, Italy.
[h]INO-CNR, Largo Fermi 6, Firenze, 50125, Italy.
[i]Dipartimento di Scienze Chimiche della Vita e della Sostenibilità Ambientale, Parco area delle Scienze 17/A Parma (PR). Email: andrea.lapini@unipr.it

† Electronic Supplementary Information (ESI) available: it includes the full acquired pump-probe and 2D electronic spectroscopy data, wavelet analysis and full description of the theoretical modeling. See DOI: 00.0000/00000000.

erties for photonic, optoelectronic and bioimaging applications. The reason for these outstanding properties lies in the balance between intermolecular van der Waals interactions and environment fluctuations, allowing for the formation of highly delocalised excitonic states,[13–18] capable of transporting energy throughout the system in an extremely fast and efficient manner.

Here we considered LHNs whose monomeric unit is the well studied C8S3 cyanine. When dispersed in water, the monomers are able to self-assemble in highly ordered double walled nanotubes of 12 nanometers lateral dimensions and longitudinal dimensions up to microns, well characterized in the past by transmission electron microscopy (TEM) and atomic force microscopy (AFM).[19–21] The possibility of controlling the morphology of the nanotube and therefore the exciton migration, is a challenging goal, still limited by the difficulty to model the structure and the dynamics of such a complex system.[22–31] Despite the amount of research work carried out in the last two decades on these LHNs,[19,20,32–41] there are still fundamental open questions related to exciton properties, mostly due to the intrinsic instability of these materials,[11,42] which prevents a thorough spectroscopic characterization.

Here we present the results of broadband femtosecond pump-probe and 2D experiments on sugar-matrix stabilized LHNs at cryogenic temperatures, carried out by significantly reducing photo-degradation and exciton annihilation. These conditions are realized using a specific sample holder, consisting in a cold finger cryostat kept under continuous transnational movement through a stepper motor, controlled by an home-written software.See SI† for further details The cryostat is hold through a specifically designed rigid frame, which allows for an almost complete suppression of the mechanical vibrations caused by the motor.

Combining low temperature and accurate control upon the sample preparation, such that nanotube bundle formation was completely avoided, we achieved a material with very low inhomogeneous disorder that, when excited with ultrafast broadband pulses, revealed the emerging of intense modulations of the transient absorption signal lasting tens of picoseconds. Furthermore, clear evidence of energy transfer between "outer wall" and "inner wall" exciton states was obtained from broad-band pump-probe spectra in agreement with literature. An ad hoc computational strategy have been developed, which allowed us to interpret the transient absorption kinetics of LHNs accounting for electronic energy transfer (EET) between the inner and outer wall of the nanotubes, to adequately reproduce the experimental results, and to provide important insights about the excited state relaxation of this complex system. Kinetic traces describing the time-evolution of the system were then fitted using an analytical function, parameterized on the basis of the introduced theoretical model. The results showed an exceptional agreement among simulated and experimental traces, which allowed to extract the energy transfer rate as a function of temperature.

Finally, temperature influence upon the time scale of energy transfer between "outer" and "inner" exciton states was characterized by recording 2D coherent spectra as a function of population time at 100K and 200K. The measurement allowed us to confirm that the two walls are weakly coupled, which results in energy transfer with a strongly temperature-dependent time constant, in fully agreement with pump-probe results and previous literature.[32,35,36,43]

2 Results and discussion

2.1 Linear spectroscopy

Linear absorption and emission spectra are reported in Fig. 1a for C8S3 monomers dissolved in methanol (blue and green lines) and for aggregate double-walled nanotube samples immobilized in a cryo-protectant sugar matrix (violet and red lines). Negligible spectral differences are observed for aggregates stabilized in the sugar matrix with respect to the solution.

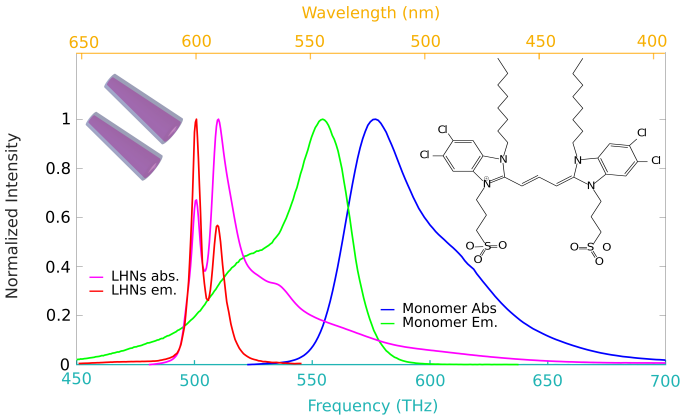

Fig. 1 *Linear absorption and emission spectra of the monomer dissolved in methanol and of the nanotubes sample in sugar matrix. The chemical structure of the monomer and a schematic representation of the LHNs are also present on top.*

The C8S3 monomer has an absorption band peaked at 580 THz, and a broad emission with a Stokes shift of 30 THz. Nanotube formation leads to a red-shift of 80 THz in the linear absorption spectrum, indicating the presence of J-type aggregation.[15,16,20,22,30] The aggregate absorption spectrum presents two main peaks centered at 500 THz and 510 THz, which have been attributed in previous literature to the inner and outer wall absorption.[21] Other three overlapping spectral features (centered at 520, 530 and 540 THz) have been assigned to outer wall contributions as well. The long tail on the blue side of the spectrum indicates the presence of a small amount of dye monomers spread in solution. The pronounced narrowing of the absorption spectrum occurring upon aggregation is an indication of delocalized excitonic behavior.[42] Two narrow peaks are observed in the emission spectrum, centered at 500 and 510 THz, respectively ascribed to the inner and outer wall fluorescence. No Stokes shift is observed between the absorption and emission spectra of the nanotubes, suggesting weak coupling with the local environment and the almost complete absence of low-energy trap states. These observations reinforce the assumption of a very low disorder in the nanotube supramolecular structure.[21]

2.2 Temperature dependent transient absorption spectroscopy

LHNs were prepared according to a previously reported procedure[42] as described in the experimental section and immobilized in a cryo-protectant sugar matrix following the method described in[41,42]. All measurements were performed on highly homogeneous 100 μm thin films.

Temperature dependent transient absorption measurements (for experimental details see section S1 of SI†) were performed on the matrix immobilized LHNs films for temperatures ranging from 80K to 260K, varied with increasing steps of 20K. The sample was excited with an ultrashort broadband laser pulse ($< 20 fs$) and the transient response was collected up to a pump-probe time delay of 20 ps. The pulse density was set below 20 $\mu J/cm^2$, implying less than one photon absorbed every 120 monomers, in order to minimize exciton-exciton annihilation (EEA) phenomena, in agreement with literature data.[23,37] Pump-probe measurements at different excitation powers were carried out in order to confirm the absence of EEA (see Fig. S19 in SI†). Such low power densities also ensure the photostability of the sample, which indeed doesn't show any typical sign of photodegradation in the transient and stationary spectral features (generally observed in terms of decreasing absorption intensity in the visible spectral region over time and blueshift of the absorption bands[41,42]).

Fig. 2 shows the normalized transient spectra recorded at 2 ps pump-probe delay at the different temperatures , together with the experimental spectrum of the NOPA output (excitation beam) on top. As noticeable, uniform excitation is applied over the probed frequency window, containing both inner and outer wall absorption. As previously reported,[37] the spectra show two negative signals, attributed to the convolution of ground state bleaching (GSB) and stimulated emission (SE) of the inner and outer walls, and two blue shifted excited state absorption (ESA) positive bands. As the temperature decreases from 260K to 80K, the entire spectrum experiences a blue shift and band narrowing, showing the same trend already observed in case of steady state absorption and emission spectra,[42] reprinted from ref [42] in Fig. S5 of SI. This behavior has been attributed to the decreasing of inhomogeneous broadening, which enables the observation of the temperature-dependent homogeneous line-narrowing. The temperature dependent spectral behavior indicates an increased exciton coupling at low temperature,[41,42] suggesting that ultrafast exciton migration occurs in terms of wave-packet-like coherent motion rather than incoherent hopping.[44]

Fig. 3a) and b) show the recorded time-frequency maps at two selected temperatures, 80K and 240K, zoomed over a time window of 5ps. The transient spectrum recorded at 2ps pump-probe delay is reported above the maps, showing two negative peaks, centered at 499 THz and 506 THz at 80K (497 and 503 THz at 240K) assigned, as previously mentioned, to the convolution of ground state bleaching and stimulated emission of the inner (low frequency band) and outer wall (high frequency band), and two blue shifted positive bands attributed to excited state absorption.

The kinetic traces obtained by averaging the transient signal over a frequency interval of 1 THz around the peaks of the inner wall (499 THz at 80K and 497 THz at 240K, red lines) and outer wall (506 THz at 80K and 503 THz at 240K, blue lines) GSB/SE are shown on the right side of the maps.

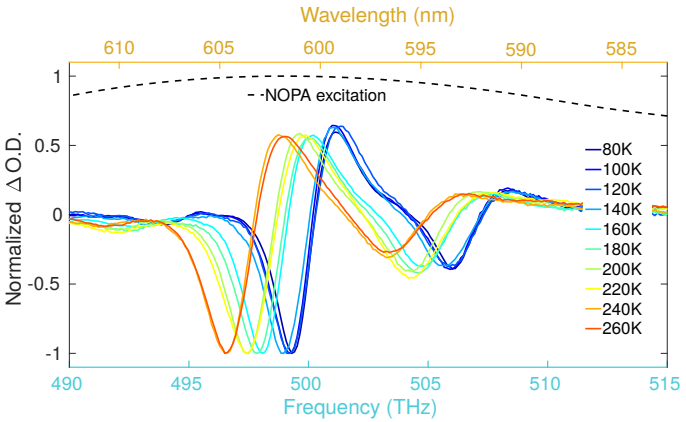

Fig. 2 *Transient spectra recorded at 2 ps pump-probe time delay at different temperatures. NOPA spectrum is plotted in dashed black line*

Comparing the kinetic traces of inner and outer walls highlights a faster decay of the outer wall signal at both temperatures, confirming the occurrence of energy transfer towards the lower energy inner wall, as observed in previous works,[24,32,34,37] also evidenced by the global analysis of the transient data reported in SI and by the growth of the cross-peak in 2D spectra reported in Fig. 8d, further discussed in section 4. This is better noticed at the higher temperature (see Fig. 3b, collected at 240 K), since at cryogenic temperature the faster decay of the outer wall is partially masked by the presence of intense in-phase oscillations, which are particularly evident on the negative (GSB/SE) bands of both inner and outer walls and on the ESA band of the inner wall (see Fig. 3a, collected at 80 K). The kinetic traces taken on the negative bands indeed show three strong and sharp oscillations on the short timescale, which are suddenly damped within the first picosecond delay and represent a 30% amplitude modulation of the total intensity of the signal. On a timescale >1ps these three intense oscillations are replaced by a broader feature, representing an oscillation at lower frequency, which remains visible over the entire acquisition timescale (full kinetic traces in SI†).

In order to rule out the possibility that the observed behavior results from experimental artefacts, we performed a test measurement on a Rodhamine B sample immobilized in a sugar matrix at 100 K, using the same experimental conditions as for LHNs. The kinetic traces registered in this case are quite different from those observed for LHNs, and present rapidly damped oscillations, assigned in terms of impulsively excited vibrations similarly observed for various dyes when excited with ultrashort laser pulses[3,45,46] (see the SI† section S3.5 for details).

Wavelet analysis[47] (Fig. S16 of SI†) was carried out on the kinetic traces measured at the negative peak (GSB/SE) of the inner and outer wall as a function of temperature, to extract the frequency of the observed oscillations, by using the protocol described by Lapini *et al.*[48] The analysis evidenced the presence of three main oscillation frequencies, with different damping times. The higher frequency mode, 130 cm^{-1}, results in a narrow fea-

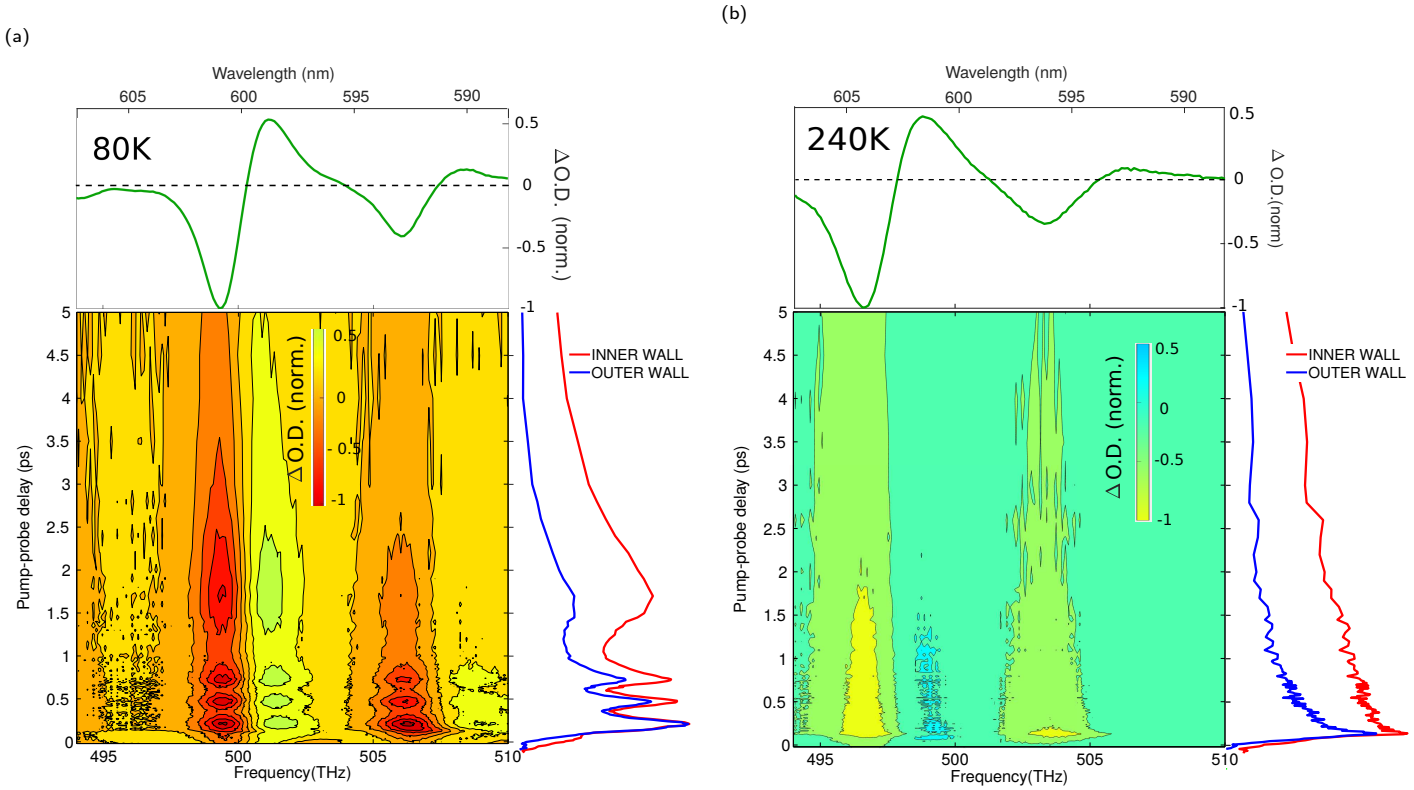

Fig. 3 *Time-frequency maps collected after broadband excitation within a time window of 5 ps, at (a) 80K and (b) 240K. On top of the maps transient spectra recorded at 2 ps pump-probe time delay are shown. On the right of the maps two kinetic traces, recorded at the negative peak (GSB/SE) of inner (499 THz at 80K and 497 THz at 240K) and outer wall (506 THz at 80K and 503 THz at 240K), are shown.*

ture in the wavelet spectrum, and dominates the kinetics within the first hundreds of femtoseconds. Upon its damping, a second less intense mode of 80 cm^{-1} frequency is observed, associated to the bumps starting over 1 ps. Subsequently, a third broad frequency component is observed, centered at around 40 cm^{-1} which lasts for a few picoseconds. Finally, a very broad and low frequency band below 30 cm^{-1} seems to modulate the excited state kinetics beyond 10 ps. This oscillatory behavior is observed as a function of temperature until 220 K (complete data in SI†). The amplitude of the modulations is reduced as the temperature increases, while no significant frequency change is observed over the probed temperature range, as confirmed by wavelet analysis. Above 220K, the oscillations are no more visible and the excited state dynamics follow a multi-exponential decay, as noticeable by looking at Fig. 3b, collected at 240 K.

As shown by the pump-probe spectra collected at various temperatures and reported in SI, the oscillations are progressively dumped as the temperature increases, and are no longer observable at room temperature (RT). We attribute this quenching to the increased dynamic disorder and experimental noise caused by the higher sample instability at RT.

2.3 Theoretical analysis

In order to understand the origin of the oscillatory transients and the mechanism of their damping in the pump-probe signals of the LHNs at low temperature, we begin from developing a reduced model describing the optical response of a single LHN. The corresponding model Hamiltonian comprises an electronic ground state, a pair of non-adiabatically coupled low-energy excited electronic states, and a single Frank-Condon-active harmonic vibrational mode. The essential aspect of this model is that the electronic energy difference between the bright and the dark states, ΔE, matches the frequency of the Franck-Condon-active mode, ω_{vib}, almost perfectly, *i.e.* $\Delta E \approx \omega_{vib}$. This results in resonant enhancement of all pump-probe transients featuring this mode (see Ref.[49] for a general discussion). Further, we assume that one of the excited electronic states is optically bright, while the other is optically dark. As is well known, dark twisted intramolecular charge-transfer (TICT) states controlled by the conical intersections are essential in photophysics of monomeric cyanines [50,51]. In addition, the involvement of dark electronic states in the LHNs excited state dynamics was previously postulated in Ref.[32], where narrow band excitation pump-probe experiments were performed at cryogenic temperature.

The interaction of the LHN with the pump and probe pulses is treated in the dipole approximation and the optically-driven LHN dynamics are described by the master equation formalism. The detailed mathematical derivation of the model is reported in section S4 of SI Models of this kind are common for the phenomenological description of vibrational coherent effects, electronic nonadiabatic couplings and vibrational relaxation/dephasing in various systems[52–55] including electron trans-

fer donor-acceptor systems [56] and organic interfaces.[57] Due to the enormous complexity and multidimensionality of the LHN system, we cannot give a microscopic underpinning or parameterization of the model Hamiltonian. The validity of this reduced description is verified *a posteriori*, since it gives a clear and insightful interpretation of the experimental signals. See also Refs.[7,26,58] for the construction of microscopic multidimensional models of optical responses of molecular aggregates.

The single nanotube model is further improved by taking into account the interaction between the inner and outer LHNs in a more phenomenological way (see Ref.[59] for the alternative approach). First, we restrict ourselves to the consideration of the GSB and SE contributions only, because the ESA contribution is caused by a simultaneous excitation of both inner- and outer-wall LHNs. Second, we notice that the experimental results of the present work do not show any signatures of electronically coherent energy transfer between the two walls: on the contrary, irreversible population transfer from the outer to the inner wall is observed. We thus chose to model this transfer process phenomenologically, by introducing the corresponding outer-to-inner energy transfer rate γ. This level of description allows us to express the signal of the coupled inner-outer LHNs system in terms of the signals of individual inner and outer walls. This consideration, as demonstrated below, permits us to get extra insight into the spectroscopic signatures of the outer-inner energy transfer. The mathematical derivation (see SI†) brings us to the following expressions for the transient-absorption pump-probe signal of the outer wall

$$S^{(o)}(t,\omega) \approx S^{(o)}_{GSB}(t,\omega) + S^{(o)}_{SE}(t,\omega)e^{-\gamma t}. \qquad (1)$$

and of the inner wall

$$S^{(i)}(t,\omega) \approx S^{(i)}_{GSB}(t,\omega) + S^{(i)}_{SE}(t,\omega)(1+\sigma(1-e^{-\gamma t})). \qquad (2)$$

Here the dimensionless parameter σ is the ratio of the initial populations of the outer and inner walls induced by the pump pulse and the subscripts GSB and SE label the corresponding contributions to the transient absorption signal obtained without inter-outer coupling ($\gamma = 0$). Eqs. (1) and (2) are the main theoretical results of the present section. They demonstrate how the transient absorption signals of individual walls ($\gamma = 0$) are related to the corresponding signals of the coupled LHNs ($\gamma \neq 0$).

In the simulations shown below, the vibrational frequency is set to $\omega^{(a)}_{vib} = 0.0153$ eV (123.5 cm^{-1}), so that the fundamental vibrational period, $2\pi/\omega^{(a)}_{vib} = 270$ fs matches the period of the vibrational oscillations observed in the transient absorption signals (see below). The other model parameters chosen for the simulations are listed in SI†. Vibrational dissipation and dephasing are described by multistate Redfield theory,[56,60] the master equation for the time evolution of the reduced system density matrix is numerically integrated in the presence of the fields of the pump and probe pulses, and the transient-absorption pump-probe signal is evaluated via the two-pulse equation-of-motion phase-matching approach as explained in Refs.[52,61,62].

The level of agreement between the experiment and the present theory can be understood from Fig. 4 where cuts of transient absorption spectra of inner (a) and outer (b) walls at 80 K are shown. Black lines correspond to experimental results and green lines correspond to the simulations described above. The simulated signals exhibit behaviors which are typical for this class of models[52,62] and their dynamical features can be straightforwardly attributed to specific processes. Oscillations with a period of 270 fs reveal the vibrational wavepacket motion. A hump around 1.5 ps, which is much more pronounced in panel (a) than in panel (b), is a signature of the electronic revival[52,62], which is caused by the coupling $\Delta^{(a)}$ of the bright and dark electronic states of each of the LHNs.

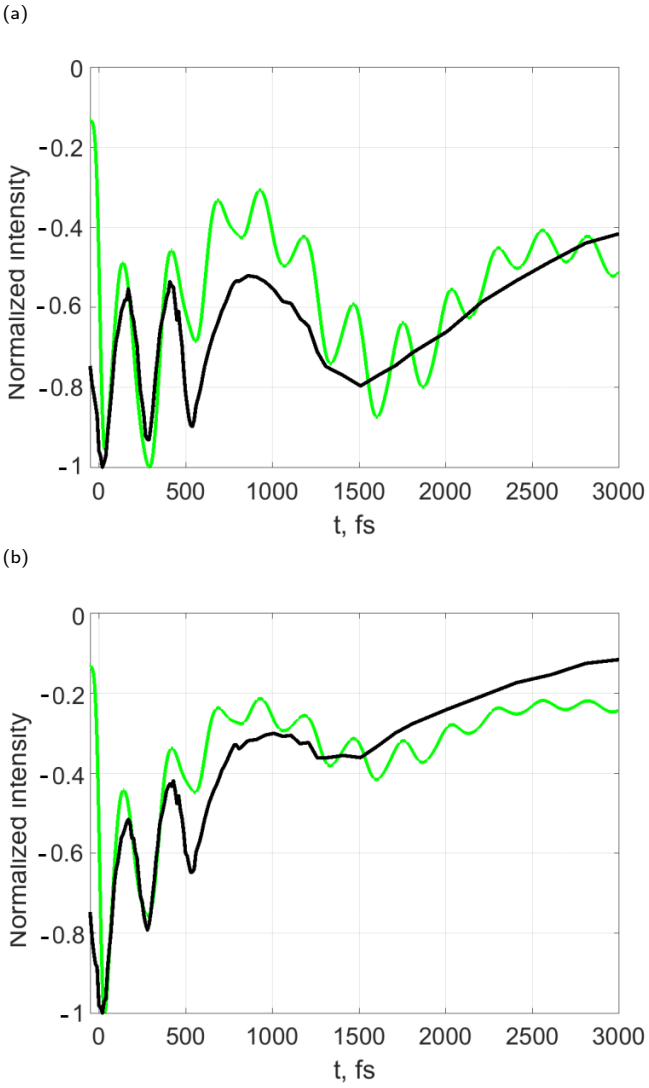

Fig. 4 *Cuts of transient absorption spectra of inner (a) and outer (b) wall at 80 K. Black lines: experimental results. Green lines: simulations. $\gamma = 0.0015$eV (12 cm^{-1}).*

Thus the following picture of the population transfer in the single LHN emerges. The vibrational wavepacket created by the pump pulse in the bright electronic state moves to the dark electronic state and (partially) returns to the bright state. These repeated wavepacket excursions are accompanied by the gradual population transfer from the bright state to the dark state, and

are manifested in the SE contribution to the pump-probe signal through the damped vibrational oscillations with a period of 270 fs. At this stage of the signal evolution, the electronic coupling $\Delta^{(a)}$ acts as a connector between the bright and dark states which is responsible for the population transfer. The rate of this process, according to Fermi's golden rule, is proportional to $\Delta^{(a)}$ squared. After a series of back and forth wavepacket motions, a coherent nature of the electronic coupling emerges. It is responsible for the electronic recurrence of the SE signal at $t = 2\pi/\Omega_R^{(a)}$. This recurrence is similar to the celebrated Rabi-beating in two-level systems. In the present case, however, Rabi frequency $\Omega_R^{(a)} \sim \Delta^{(a)}$ is renormalized by the vibrational parameters of the model. Nevertheless, the assumption $\Omega_R^{(a)} = \Delta^{(a)}$ yields Rabi period $2\pi/\Omega_R^{(a)} = 1.6$ ps which matches, accidentally, the position of the hump quite well. The outer-to-inner wall energy transfer time $\gamma^{-1} = 439$ fs allows us to simultaneously describe the inner and outer wall kinetics, which lands additional support to the theory developed in the previous section.

In order to corroborate our model, and provide a better understanding of its underlying physics we have tried to shed light on the origin of the the vibrational motion at 123.5 cm^{-1}. To the aim, we have performed an analysis of the Franck-Condon (FC) active vibrational modes in the ground to first excited singlet transition of the CS83 monomer unit, using well known computational methodologies based on geometry optimization of the two electronic states followed by the calculation of the so-called Duschinsky normal mode transformation.[63–66]. The results of the analysis, which are given in SI, show the existence of two vibrational modes with frequencies 117 cm^{-1} and 131 cm^{-1} having a moderate FC activity. The average frequency of this two vibrations matches very closely the observed 125.5 cm^{-1} of the effecive mode used in our simulations. While it is not possible to rule out the existence of other nuclear vibrations having a similar frequency and belonging to the nanotube aggregate, our theoretical analysis clearly suggests that the modes responsible for the observed quantum beatings belong to the the monomer unit, thus providing a clear physical picture of the photophysics of the system.

The simple three-electronic-states single-vibrational-mode model developed above allows to grasp all the substantial features in the detected transient absorption signals and to pinpoint their origins. Nevertheless, the agreement is far from being quantitative. For example, absolutely unsurprisingly, the model overemphasizes the amplitude of vibrational oscillations. Accounting for static disorder in the electronic excitation energies of our model does not significantly improve the results, limiting its applicability for a quantitative interpretation of the experimental signals. Nonetheless, this model can be used for developing a tailored fitting procedure which can be conveniently used for the quantitative analysis of the experimental signals. On this basis, we constructed an analytical fitting function (mathematical details in SI†) of the negative peaks (GSB/SE) kinetic traces, where the different parameters can be interpreted in terms of the model parameters described in the previous section.

The results of the fit via Eq. S23 (SI†) for 100 K and 200 K are

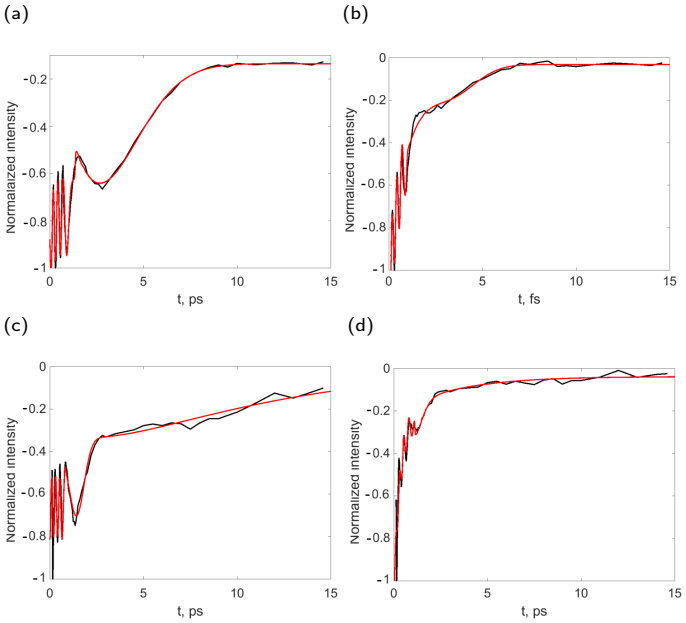

Fig. 5 *Cuts of transient absorption spectra of inner (left) and outer (right) wall at 100 K (top) and 200 K (bottom). Black lines: experimental results. Red lines: fit via eq. S23 (SI†).*

presented in Fig. 5. As noticeable, the fitting function accurately reproduces the experimental data. It describes both the structured kinetics of the inner wall with vibrational oscillations and a pronounced electronic revival as well as less-featured and faster decaying outer wall response. It should be pointed out that vibrational oscillations, sometimes enhanced by resonant electron-vibrational coupling effects, have been detected in femtosecond nonlinear signals of molecular aggregates [67] and LHN systems.[35,37] However, predominantly electronic coherences were detected in transient-absorption[68] and photoelectron[69] pump-probe signals of fluorinated benzenes, in transient absorption signals of dye-semiconductor complexes [70,71] as well as in electronic 2D signals of molecular aggregates consisting of several (from two up to a few dozens) monomers.[72] Biological significance of electronic coherent effects in photosynthetic light harvesting has nowadays been questioned [73,74]. However, unequivocal detection of the electronic coherent recurrence on a time scale of ~ 1.5 ps in the transient-absorption pump-probe signal of the double-wall LHNs system consisting of many thousands of cyanine dyes is a remarkable and fairly unexpected result of the present work.

In order to get insight on the inter-walls coupling, the fit procedure was performed by optimizing the function parameters for each temperature, with the only constrain on the ET rate, set as the same for inner and outer wall kinetics. The plot of the ET time-constant γ, corresponding to the model parameter a_{12} in eq. S23 (SI†), as a function of temperature, is reported in Fig. 6c. The ET speeds up as the temperature increases, with a time-constant ranging from 0.95 ps at 80K to 0.4 ps at 260K. This result is consistent with previous assumption of weak coupling between the walls, and consequent ET favoured by temperature fluctuations.[42]

Fig. 7 shows a schematic representation of the energetic levels

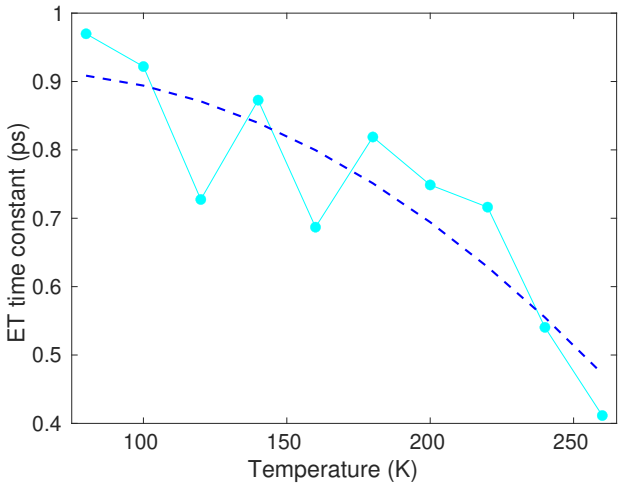

Fig. 6 *ET time-constant, obtained as the fitting parameter a_{12} in eq. S23 (SI†) as a function of temperature. The dashed blue line indicates the decrease trend.*

involved in the observed excited state dynamics at cryogenic temperature, with two electronic states modeled for each nanotube wall: ultrafast excitation populates the bright states, higher in energy compared to the dark states. In the process of excited state relaxation, both SE and ESA bands are modulated by population exchange between bright and dark states, which causes strong oscillations at short pump-probe delays and the electronic revivals observed after a few picoseconds. Energy transfer between the outer and inner wall occurs within the first picosecond, and it is responsible for the observed faster ground state recovery of the outer wall. As already mentioned, at high temperatures the thermal bath fluctuations dominate over the electronic coupling between dark and bright states, and the oscillatory behavior is suppressed, nevertheless the state diagram remains the same as depicted in Fig. 7. The predominance of dynamic disorder is also confirmed by the previously discussed red shift of the transient spectra, that evidence a reduction of the exciton delocalization extent.

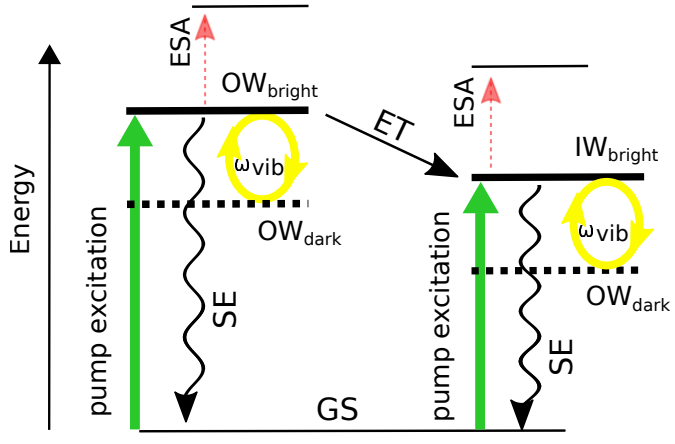

Fig. 7 *Schematic representation of the energetic levels involved in the ultrafast excited state dynamics of LHNs nanotubes at cryogenic temperature.*

2.4 2D electronic spectroscopy

To further characterize electronic energy transfer (EET), we recorded the excitation spectra of the aggregate, by selectively monitoring the fluorescence of the inner wall at 500 THz. The excitation spectrum is reported in Fig. 8a together with the linear absorption spectrum of the nanotube. The comparison between absorption and excitation spectra clearly reveals a contribution coming from the outer wall to the fluorescence of the inner wall. This result further confirms the presence of weak electronic coupling between the two walls, leading to EET, as already stated in literature.[37,42]

To investigate the electronic interactions between inner and outer wall in more detail, 2D electronic spectra were furthermore collected at two different temperatures, using the setup described in section S1 of SI†. The 2D maps in Fig. 8b,c, recorded at 100K and 260K respectively, show the typical GSB/SE peaks of inner and outer wall on the diagonal (yellow), together with blue shifted positive ESA bands (blue). The maps recorded at a population time of 700 fs further show the presence of an elongated cross peak, rising in time when exciting the outer wall around 510 THz and probing the inner wall third order response at around 500 THz. The intensity of the cross peak as a function of the population time is plotted in Fig. 8d at the two analyzed temperatures, together with polynomial fits (linear and quadratic fits at 100K and 200K, respectively) to help following the trend. At 100 K the cross peak intensity increases linearly within the experimental timescale (until 1350 fs), indicating that energy transfer occurs on a longer timescale. On the contrary, at 260K the intensity reaches a plateau below 1 ps, suggesting that EET occurs within this time frame. These results are in very good agreement with the EET rates extracted from pump-probe measurements (0.93 ps at 100K and 0.4 ps at 260K), and further confirm weak coupling among the outer and inner walls of the nanotubes.

3 Conclusion

In summary, we analyzed the time-resolved spectroscopic behavior of C8S3 light harvesting nanotubes embedded in a sugar matrix, proving the presence of new transient spectral features and analyzing the exciton behavior at cryogenic temperatures.

To the best of our knowledge, the peculiar oscillatory pattern displayed by the kinetic traces recorded at low temperature, which exhibit several vibrational oscillations and an electronic recurrence, has not been previously observed. The experimental observations reported in this work result from a high degree of order and stability of LHNs, achieved by highly controlled experimental conditions, minimized annihilation and photo-degradation.

The excited state dynamics are rationalized within an effective LHN model based on the Redfield theory of exciton delocalization. The simulations revealed that the observed oscillatory features result from the presence of coupled dark and bright states, whose interaction leads to the observed intensity modulation in the transient signal. This theoretical framework allowed us to simulate the pump-probe signals and investigate the energy transfer between the two walls of the nanotube.

A quantitative fit of the kinetic traces was obtained using an analytical function, inspired by the theoretical model previously

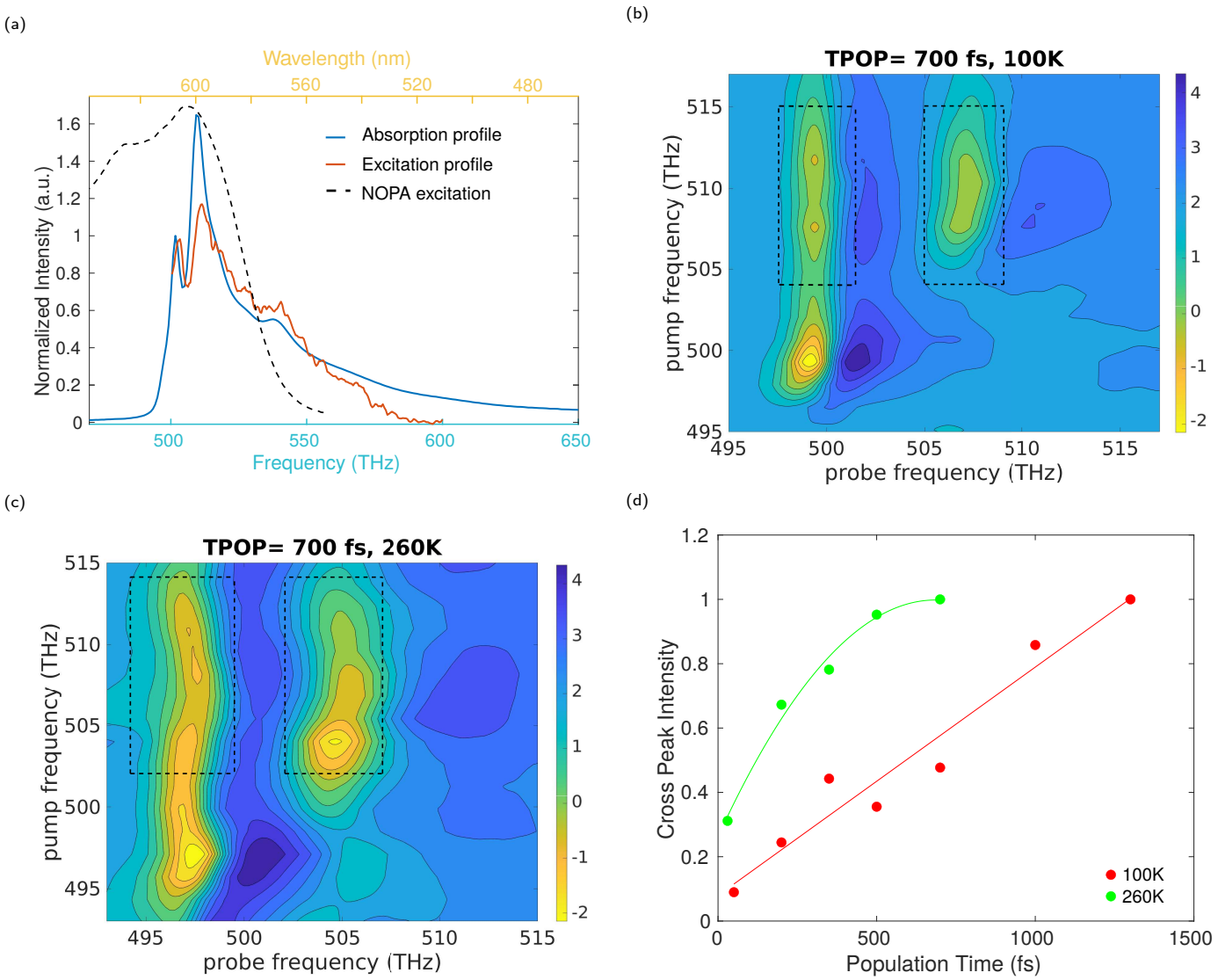

Fig. 8 *a) Linear absorption and excitation (emission collected at 500 THz) spectra of the LHNs sample in sugar matrix. Dashed black curve indicates the experimental spectrum of the NOPA. b) 2DES maps collected at 100K and 700 fs population time, showing two negative diagonal peaks centered at 503 THz and 512 THz, representing the bleaching signal of inner and outer wall, and a negative cross-peak at pump frequency 512 THz and probe frequency 503 THz, confirming the presence of outer-to-inner wall energy transfer; positive bands on the blue edge of the negative components are the ESA signals. Black dashed rectangles indicate the cross peak (lower probe frequency) and outer wall bleaching (higher probe frequency) areas where the signal is averaged to obtain the cross peak intensity plot in panel (d). c) 2DES maps collected at 260K and 700 fs population time, showing the spectral evolution of the inner and outer wall GSB and ESA, and of the cross-peak. Black dashed rectangles indicate the cross peak (lower probe frequency) and outer wall bleaching (higher probe frequency) areas where the signal is averaged to obtain the cross peak intensity plot in panel (d). d) Cross peak intensity, normalized for the signal at the excitation energy (outer wall GSB), plotted as a function of population time at 100K (green line) and 260K (green line), using the maps recorded aa a function of the population time (see section S5 in SI†); the kinetics at the two temperatures are notably different: the higher is the temperature, the faster is the energy transfer. The solid lines indicate a quadratic fit performed on the experimental data.*

described. Besides the exceptional agreement between the fit and the recorded kinetic traces, the fitting procedure allowed to extract the energy transfer rate as a function of temperature, which showed a good agreement with the experimental rate obtained from 2DES measurements carried out at different temperatures and with previous literature.

Our results shed further light on the exciton transport mechanism in self assembled aggregates of organic chromophores, whose deep understanding is a fundamental step forwards for the realization of new optical materials with improved performances.

4 Experimental section

Aggregate preparation was carried out from 3,3-bis(2-sulfopropyl)-5,5',6,6'-tetrachloro-1,1'- dioctylbenzimidacarbocyanine (C8S3) molecules following ref.[42]: a solution 10^{-3} mM of the C8S3 amphiphilic monomer in methanol is mixed with water in 30:70 v/v ratio. Aggregates assemble into nanotubular structures, consisting in two cylindrical walls arranged concentrically (inner wall and outer wall of 6 nm and 12 nm

radius, respectively), previously characterized in details by spectroscopic, theoretical and microscopy approach.[12,20–22,40] The nanotubes form over 24 hours, afterwards they are incorporated in a sugar matrix obtained by a saturated solution of sucrose and trehalose in water. The paste is then spread on a demountable quartz cell with 100 μm optical path, and left to dry in vacuum (0.5 atm) up to 48 hours, in order to obtain a stable sample.[41,42]

Linear absorption and emission spectra were recorded using a Perkin Elmer Lambda950 spectrometer and a Perkin Elmer LS55 fluorimeter.

For ultrafast transient absorption spectroscopy (TAS) and 2D electronic spectroscopy (2DES) measurements, we used a modified version of the setup described in[75]. Briefly, ultrafast pulses coming from the master oscillator Coherent MICRA are amplified by the regenerative amplifier Coherent Legend Elite, and then sent to the Non-Collinear Optical Amplifier (NOPA), which produces ultrafast pulses tunable between 500 and 800 nm, compressed by means of a couple of chirped mirrors. After pump-probe separation performed by a beam splitter, a novel implementation of the 2D setup allows the generation of two collinear pump pulses with very good phase difference stability, allowing to get purely absorpitive 2D spectra in the pseudo-pump-probe geometry. Further experimental details of the spectroscopic setup are reported in section S1 of SI.

Ultrafast broadband pump-probe and 2D electronic spectroscopy at cryogenic temperatures were carried out using a liquid nitrogen flow cryostat, kept under continuous periodic translational motion by means of a stepper motor controlled by home-made electronic equipment to prevent photo-damage of the sample. A rigid frame allows holding the cryostat to the optical table, isolating the sample from the mechanical vibrations caused by translation of the cryostat. A picture of the cryostat in the setup is shown in picture S4 of SI†. At the best of our knowledge, a similar equipment has not been previously used. Temperature control was achieved by means of a Lakeshore 330 system and the temperature was monitored by means of a silicon diode fixed on the cell close to the sample.

Author Contributions

Sandra Doria: Conceptualization, Data curation, Formal Analysis, Investigation, Validation, Visualization, Writing - original draft, Writing - review and editing; **Mariangela Di Donato**: Data Curation, Funding Acquisition, Investigation, Resources, Supervision, Writing - original draft, Writing - review and editing; **Raffaele Borrelli**: Investigation, Methodology, Software; **Maxim F. Gelin**: Investigation, Methodology, Software; **Justin Caram**: Conceptualization; **Marco Pagliai**: Data curation, Formal analysis; **Paolo Foggi**: Funding acquisition, Supervision; **Andrea Lapini**: Conceptualization, Data curation, Investigation, Project administration, Supervision, Validation, Writing - original draft, Writing - review and editing.

Conflicts of interest

There are no conflicts to declare.

Acknowledgements

The authors thank the European Union's Horizon 2020 research and innovation program under grant agreement n. 871124 Laserlab-Europe.

R.B acknowledges funding from the European Union's Horizon 2020 Research and Innovation Program under Grant Agreement No. 826013.

M. F. G. acknowledges support from the Hangzhou Dianzi University through startup funding.

Notes and references

1 Q. Zhang, T. Atay, J. R. Tischler, M. S. Bradley, V. Bulović and A. V. Nurmikko, *Nature Nanotechnology*, 2007, **2**, 555–559.

2 F. S. Freyria, J. M. Cordero, J. R. Caram, S. Doria, A. Dodin, Y. Chen, A. P. Willard and M. G. Bawendi, *Nano Letters*, 2017, **17**, 7665–7674.

3 T.-S. Yang, M.-S. Chang, R. Chang, M. Hayashi, S. H. Lin, P. Vöhringer, W. Dietz and N. F. Scherer, *The Journal of Chemical Physics*, 1999, **110**, 12070–12081.

4 O. Ostroverkhova, *Chemical Reviews*, 2016, **116**, 13279–13412.

5 S. Kéna-Cohen, M. Davanço and S. R. Forrest, *Phys. Rev. Lett.*, 2008, **101**, 116401.

6 S. Kéna-Cohen and S. R. Forrest, *Nature Photonics*, 2010, **4**, 371–375.

7 N. J. Hestand and F. C. Spano, *Chemical Reviews*, 2018, **118**, 7069–7163.

8 A. Proppe, Y. Li, A. Aspuru-Guzik and et al, *Nat Rev Mater*, 2020, **5**, 828–846.

9 K. Kreger, H.-W. Schmidt and R. Hildner, *Electronic Structure*, 2021, **3**, 023001.

10 T. Kim, S. Ham, S. H. Lee, Y. Hong and D. Kim, *Nanoscale*, 2018, **10**, 16438–16446.

11 B. Kriete, C. J. Feenstra and M. S. Pshenichnikov, *Phys. Chem. Chem. Phys.*, 2020, **22**, 10179–10188.

12 D. M. Eisele, D. H. Arias, X. Fu, E. A. Bloemsma, C. P. Steiner, R. A. Jensen, P. Rebentrost, H. Eisele, A. Tokmakoff, S. Lloyd, K. A. Nelson, D. Nicastro, J. Knoester and M. G. Bawendi, *Proceedings of the National Academy of Sciences*, 2014, **111**, E3367–E3375.

13 F. Würthner, T. E. Kaiser and C. R. Saha-Möller, *Angewandte Chemie International Edition*, 2011, **50**, 3376–3410.

14 K. Stefan and D. Siegfried, *International Journal of Photoenergy*, 2006, **2006**,.

15 H. v. Berlepsch, K. Ludwig, S. Kirstein and C. Böttcher, *Chemical Physics*, 2011, **385**, 27 – 34.

16 E. K. Walker, D. A. Vanden Bout and K. J. Stevenson, *The Journal of Physical Chemistry C*, 2011, **115**, 2470–2475.

17 N. Katayama, S. Enomoto, T. Sato, Y. Ozaki and N. Kuramoto, *The Journal of Physical Chemistry*, 1993, **97**, 6880–6884.

18 F. C. Spano, *Accounts of Chemical Research*, 2010, **43**, 429–439.

19 A. V. Sorokin, I. Y. Ropakova, S. Wolter, R. Lange, I. Barke,

S. Speller, S. L. Yefimova, Y. V. Malyukin and S. Lochbrunner, *The Journal of Physical Chemistry C*, 2019, **123**, 9428–9444.
20 J. L. Lyon, D. M. Eisele, S. Kirstein, J. P. Rabe, D. A. Vanden Bout and K. J. Stevenson, *The Journal of Physical Chemistry C*, 2008, **112**, 1260–1268.
21 D. Eisele, C. Cone, E. Bloemsma, S. Vlaming, C. van der Kwaak, R. Silbey, M. Bawendi, J. Knoester, J. Rabe and D. Vanden Bout, *Nat Chem*, 2012, **4**, 655–62.
22 C. Didraga, A. Pugžlys, P. R. Hania, H. von Berlepsch, K. Duppen and J. Knoester, *The Journal of Physical Chemistry B*, 2004, **108**, 14976–14985.
23 C. Didraga, V. A. Malyshev and J. Knoester, *The Journal of Physical Chemistry B*, 2006, **110**, 18818–18827.
24 B. Kriete, J. Lüttig, T. Kunsel, P. Malý, T. L. C. Jansen, J. Knoester, T. Brixner and M. S. Pshenichnikov, *Nat Commun*, 2019, **10**, 4615.
25 F. Haverkort, A. Stradomska, A. H. de Vries and J. Knoester, *The Journal of Physical Chemistry B*, 2013, **117**, 5857–5867.
26 A. S. Bondarenko, I. Patmanidis, R. Alessandri, P. C. T. Souza, T. L. C. Jansen, A. H. de Vries, S. J. Marrink and J. Knoester, *Chem. Sci.*, 2020, **11**, 11514–11524.
27 P. W. J. M. Frederix, I. Patmanidis and S. J. Marrink, *Chem. Soc. Rev.*, 2018, **47**, 3470–3489.
28 I. Patmanidis, A. H. de Vries, T. A. Wassenaar, W. Wang, G. Portale and S. J. Marrink, *Phys. Chem. Chem. Phys.*, 2020, **22**, 21083–21093.
29 K. J., *International Journal of Photoenergy*, 2006, **2006**, 10.
30 A. S. Bondarenko, T. L. C. Jansen and J. Knoester, *The Journal of Chemical Physics*, 2020, **152**, 194302.
31 C. Chuang, J. Knoester and J. Cao, *The Journal of Physical Chemistry B*, 2014, **118**, 7827–7834.
32 R. Augulis, A. Pugžlys and P. H. M. van Loosdrecht, *physica status solidi c*, 2006, **3**, 3400–3403.
33 K. A. Clark, C. W. Cone and D. A. Vanden Bout, *The Journal of Physical Chemistry C*, 2013, **117**, 26473–26481.
34 J. Yuen-Zhou, D. H. Arias, D. M. Eisele, C. P. Steiner, J. J. Krich, M. G. Bawendi, K. A. Nelson and A. Aspuru-Guzik, *ACS Nano*, 2014, **8**, 5527–5534.
35 F. Milota, V. I. Prokhorenko, T. Mancal, H. von Berlepsch, O. Bixner, H. F. Kauffmann and J. Hauer, *The Journal of Physical Chemistry A*, 2013, **117**, 6007–6014.
36 J. Sperling, A. Nemeth, J. Hauer, D. Abramavicius, S. Mukamel, H. F. Kauffmann and F. Milota, *The Journal of Physical Chemistry A*, 2010, **114**, 8179–8189.
37 R. Pandya, R. Y. S. Chen, A. Cheminal, T. Thomas, A. Thampi, A. Tanoh, J. Richter, R. Shivanna, F. Deschler, C. Schnedermann and A. Rao, *The Journal of Physical Chemistry Letters*, 2018, **9**, 5604–5611.
38 L. Lüer, S. K. Rajendran, T. Stoll, L. Ganzer, J. Rehault, D. M. Coles, D. Lidzey, T. Virgili and G. Cerullo, *The Journal of Physical Chemistry Letters*, 2017, **8**, 547–552.
39 B. Kriete, A. S. Bondarenko, R. Alessandri, I. Patmanidis, V. V. Krasnikov, T. L. C. Jansen, S. J. Marrink, J. Knoester and M. S. Pshenichnikov, *Journal of the American Chemical Society*, 2020, **142**, 18073–18085.
40 D. Eisele, J. Knoester, P. J. Kirstein, S.and Rabe and D. A. Vanden Bout, *Nature Nanotech*, 2009, **4**, 658–663.
41 S. Doria, T. S. Sinclair, N. D. Klein, D. I. G. Bennett, C. Chuang, F. S. Freyria, C. P. Steiner, P. Foggi, K. A. Nelson, J. Cao, A. Aspuru-Guzik, S. Lloyd, J. R. Caram and M. G. Bawendi, *ACS Nano*, 2018, **12**, 4556–4564.
42 J. R. Caram, S. Doria, D. M. Eisele, F. S. Freyria, T. S. Sinclair, P. Rebentrost, S. Lloyd and M. G. Bawendi, *Nano Letters*, 2016, **16**, 6808–6815.
43 A. S. Bondarenko, J. Knoester and T. L. Jansen, *Chemical Physics*, 2020, **529**, 110478.
44 I. G. Scheblykin, O. Y. Sliusarenko, L. S. Lepnev, A. G. Vitukhnovsky and M. Van der Auweraer, *The Journal of Physical Chemistry B*, 2000, **104**, 10949–10951.
45 D. Kumar Das, K. Makhal and D. Goswami, *Phys. Chem. Chem. Phys.*, 2018, **20**, 13400–13411.
46 U. Buck, *AIP Conference Proceedings*, 1993, **295**, 719–727.
47 C. Torrence and G. P. Compo, *Bull. Am. Meteorol. Soc.*, 1998, **79**, 61 – 78.
48 A. Lapini, M. Pagliai, S. Fanetti, M. Citroni, S. Scandolo, R. Bini and R. Righini, *J. Phys. Chem. Lett.*, 2016, **7**, 3579–3584.
49 M. F. Gelin, L. Chen, R. Borrelli and E. Thyrhaug, *Chem. Phys.*, 2020, **528**, 110495.
50 W. Rettig, *Angew. Chem. Int. Ed.*, 1986, **25**, 971–988.
51 S. McConnell, R. H. McKenzie and S. Olsen, *J. Chem. Phys.*, 2015, **142**, 084502.
52 D. Egorova, M. F. Gelin and W. Domcke, *The Journal of Chemical Physics*, 2005, **122**, 134504.
53 P. Malý, O. J. G. Somsen, V. I. Novoderezhkin, T. Mančal and R. van Grondelle, *ChemPhysChem*, 2016, **17**, 1356–1368.
54 X. Li, G. G. Gurzadyan, M. F. Gelin, W. Domcke, C. Gong, J. Liu and L. Sun, *The Journal of Physical Chemistry C*, 2018, **122**, 23321–23328.
55 L. Chen, M. F. Gelin, Y. Zhao and W. Domcke, *The Journal of Physical Chemistry Letters*, 2019, **10**, 5873–5880.
56 V. May and O. Kühn, in *Front Matter*, John Wiley & Sons, Ltd, 2011, pp. I–XIX.
57 M. F. X. Dorfner, S. Hutsch, R. Borrelli, M. Gelin and F. Ortmann, *J. Phys. Materials*, 2021, **532**,.
58 A. S. Bondarenko, T. L. C. Jansen and J. Knoester, *The Journal of Chemical Physics*, 2020, **152**, 194302.
59 G. Gordeev, S. Wasserroth, H. Li, B. Flavel and S. Reich, *Moiré-induced Vibrational Coupling in Double Walled Carbon Nanotubes*, 2021.
60 A. Redfield, *Advances in Magnetic Resonance*, Academic Press, 1965, vol. 1, pp. 1–32.
61 M. F. Gelin, D. Egorova and W. Domcke, *Accounts of Chemical Research*, 2009, **42**, 1290–1298.
62 E. Palacino-González, M. F. Gelin and W. Domcke, *The Journal of Chemical Physics*, 2019, **150**, 204102.
63 R. Borrelli and A. Peluso, *J. Chem. Phys.*, 2006, **125**, 194308.
64 R. Borrelli, A. Capobianco and A. Peluso, *Can. J. Chem.*, 2013,

91, 495–504.

65 R. Borrelli, S. Ellena and C. Barolo, *Phys. Chem. Chem. Phys.*, 2014, **16**, 2390–2398.

66 R. Borrelli and A. Peluso, *J. Chem. Theory Comput.*, 2015, **11**, 415–422.

67 A. Schubert, V. Settels, W. Liu, F. Würthner, C. Meier, R. F. Fink, S. Schindlbeck, S. Lochbrunner, B. Engels and V. Engel, *J. Phys. Chem. Lett.*, 2013, **4**, 792–796.

68 S. A. Kovalenko, A. L. Dobryakov and V. Farztdinov, *Phys. Rev. Lett.*, 2006, **96**, 068301.

69 O. Hüter, M. Sala, H. Neumann, S. Zhang, H. Studzinski, D. Egorova and F. Temps, *J. Chem. Phys.*, 2016, **145**, 014302.

70 R. Huber, J.-E. Moser, M. Grätzel and J. Wachtveitl, *J. Phys. Chem. B*, 2002, **106**, 6494.

71 J. Li, I. Kondov, H. Wang and M. Thoss, *J. Phys. Chem. C*, 2010, **114**, 18481.

72 G. D. Scholes, G. R. Fleming, L. X. Chen, A. Aspuru-Guzik, A. Buchleitner, D. F. Coker, G. S. Engel, R. Van Grondelle, A. Ishizaki, D. M. Jonas, J. S. Lundeen, J. K. McCusker, S. Mukamel, J. P. Ogilvie, A. Olaya-Castro, M. A. Ratner, F. C. Spano, B. Whaley and X. Zhu, *Nature*, 2017, **543**, 647–656.

73 J. Cao, R. Cogdell, D. Coker, H.-G. Duan, J. Hauer, U. Kleinekathöfer, T. Jansen, T. Mančal, R. Miller, J. Ogilvie, V. Prokhorenko, T. Renger, H.-S. Tan, R. Tempelaar, M. Thorwart, E. Thyrhaug, S. Westenhoff and D. Zigmantas, *Sci. Adv.*, 2020, **6**, eaaz4888.

74 T. Mančal, *Chem. Phys.*, 2020, **532**, 110663.

75 S. Doria, A. Lapini, M. Di Donato, R. Righini, N. Azzaroli, A. Iagatti, J. R. Caram, T. S. Sinclair, L. Cupellini, S. Jurinovich, B. Mennucci, G. Zanotti, A. M. Paoletti, G. Pennesi and P. Foggi, *Phys. Chem. Chem. Phys.*, 2018, **20**, 22331–22341.